

- [8] A. Yershova, L. Jaillet, T. Simeon, and S. LaValle, "Dynamic-domain RRTS: Efficient exploration by controlling the sampling domain," in *Proc. IEEE Int. Conf. Robot. Autom.*, 2005, pp. 3856–3861.
- [9] L. Zhang and D. Manocha, "An efficient retraction-based rrt planner," in *Proc. IEEE Int. Conf. Robot. Autom.*, 2008, pp. 3743–3750.
- [10] S. Rodriguez, X. Tang, J.-M. Lien, and N. M. Amato, "An obstacle-based rapidly-exploring random tree," in *Proc. IEEE Int. Conf. Robot. Autom.*, 2006, pp. 895–900.
- [11] D. Hsu, G. Sanchez-Ante, H. lun Cheng, and J.-C. Latombe, "Multi-level free-space dilation for sampling narrow passages in prm planning," in *Proc. IEEE Int. Conf. Robot. Autom.*, 2006, pp. 1255–1260.
- [12] S. Redon and M. Lin, "Practical local planning in the contact space," in *Proc. IEEE Int. Conf. Robot. Autom.*, 2005, pp. 4200–4205.
- [13] M. Saha and J.-C. Latombe, "Finding narrow passages with probabilistic roadmaps: The small step retraction method," in *Proc. Int. Conf. Intell. Robots Syst.*, 2005, pp. 622–627.
- [14] J. Lee, O. Kwon, L. Zhang, and S. Yoon, "SR-RRT: Selective retraction-based RRT planner," in *Proc. IEEE Int. Conf. Robot. Autom.*, 2012, pp. 2543–2550.
- [15] S. M. LaValle, *Planning Algorithms*. Cambridge, U.K.: Cambridge Univ. Press, 2006.
- [16] D. Hsu, J. Latombe, and H. Kurniawati, "On the probabilistic foundations of probabilistic roadmap planning," *Int. J. Robot. Res.*, vol. 25, no. 7, pp. 627–643, 2006.
- [17] J. Bruce and M. Veloso, "Real-time randomized path planning for robot navigation," in *Proc. Int. Conf. Intell. Robots Syst.*, 2002, pp. 2383–2388.
- [18] D. Ferguson, N. Kalra, and A. Stentz, "Replanning with RRTs," in *Proc. IEEE Int. Conf. Robot. Autom.*, 2006, pp. 1243–1248.
- [19] M. Branicky, M. Curtiss, J. Levine, and S. Morgan, "Sampling-based planning, control and verification of hybrid systems," *Proc. Inst. Elect., Control Theory Appl.*, vol. 153, pp. 575–590, 2006.
- [20] J. Cortes, L. Jaillet, and T. Simeon, "Molecular disassembly with RRT-like algorithms," in *Proc. IEEE Int. Conf. Robot. Autom.*, 2007, pp. 3301–3306.
- [21] B. Burns and O. Brock, "Single-query motion planning with utility-guided random trees," in *Proc. IEEE Int. Conf. Robot. Autom.*, 2007, pp. 3307–3312.
- [22] S. Lindemann and S. LaValle, "Incrementally reducing dispersion by increasing voronoi bias in RRTS," in *Proc. IEEE Int. Conf. Robot. Autom.*, 2004, pp. 3251–3257.
- [23] J. Guittou, J.-L. Farges, and R. Chatila, "Cell-RRT: Decomposing the environment for better plan," in *Proc. Int. Conf. Intell. Robots Syst.*, 2009, pp. 5776–5781.
- [24] S. Karaman and E. Frazzoli, "Sampling-based algorithms for optimal motion planning," *Int. J. Robot. Res.*, vol. 30, no. 7, pp. 846–894, 2011.
- [25] S. Rodriguez, S. Thomas, R. Pearce, and N. Amato, "RESAMPL: A region-sensitive adaptive motion planner," in *Proc. Int. Workshop Algorithm. Found. Robot.*, 2006, pp. 4037–4044.
- [26] M. Morales, L. Tapia, R. Pearce, S. Rodriguez, and N. Amato, "A machine learning approach for feature-sensitive motion planning," in *Algorithm. Found. Robot. VI*, vol. 17, Berlin, Germany: Springer, 2005, pp. 361–376.
- [27] J. Denny and N. M. Amato, "Toggle PRM: Simultaneous mapping of C-free and C-obstacle—A study in 2D," in *Proc. IEEE Int. Conf. Robot. Autom.*, 2011, pp. 2632–2639.
- [28] S. Dalibard and J. Laumond, "Linear dimensionality reduction in random motion planning," *Int. J. Robot. Res.*, vol. 30, no. 12, pp. 1461–1476, 2011.
- [29] N. Amato, O. Bayazit, L. Dale, C. Jones, and D. Vallejo, "OBPRM: An obstacle-based PRM for 3D workspaces," in *Proc. Int. Workshop Algorithm. Found. Robot.*, 1998, pp. 197–204.
- [30] V. Boor, M. Overmars, and A. van der Stappen, "The Gaussian sampling strategy for probabilistic roadmap planners," in *Proc. IEEE Int. Conf. Robot. Autom.*, 1999, pp. 1018–1023.
- [31] Z. Sun, D. Hsu, T. Jiang, H. Kurniawati, and J. Reif, "Narrow passage sampling for probabilistic roadmap planning," *IEEE Trans. Robot.*, vol. 21, no. 6, pp. 1105–1115, Dec. 2005.
- [32] H.-Y. Yeh, S. Thomas, D. Eppstein, and N. M. Amato, "UOBPRM: A uniformly distributed obstacle-based PRM," in *Proc. Int. Conf. Intell. Robots Syst.*, 2012, pp. 2653–2662.
- [33] A. Shkolnik and R. Tedrake, "Sample-based planning with volumes in configuration space," *CoRR*, 2011. Available <http://arxiv.org/abs/1109.3145>.
- [34] E. Ferre and J.-P. Laumond, "An iterative diffusion algorithm for part disassembly," in *Proc. IEEE Int. Conf. Robot. Autom.*, 2004, pp. 3149–3154.
- [35] D. Hsu, G. Sanchez-Ante, and Z. Sun, "Hybrid PRM sampling with a cost-sensitive adaptive strategy," in *Proc. IEEE Int. Conf. Robot. Autom.*, 2005, pp. 3874–3880.
- [36] I. Jolliffe, *Principle Component Analysis*. New York, NY, USA: Springer-Verlag, 1986.
- [37] D. Erdogmus, Y. N. Rao, H. Peddaneni, A. Hegde, and J. C. Principe, "Recursive principal components analysis using eigenvector matrix perturbation," *EURASIP J. Appl. Signal Process.*, vol. 2004, pp. 2034–2041, 2004.
- [38] D. Kim, J. Lee, and S. Yoon, "Cloud RRT*: Sampling cloud based RRT*," in *Proc. IEEE Int. Conf. Robot. Autom.*, 2014.
- [39] T. L. Loi, J.-P. Heo, J. Lee, and S.-E. Yoon, "VLSH: Voronoi-based locality sensitive hashing," in *Proc. Int. Conf. Intell. Robots Syst.*, 2013, pp. 2543–2550.
- [40] J. Pan, L. Zhang, and D. Manocha, "Retraction-based RRT planner for articulated models," in *Proc. IEEE Int. Conf. Robot. Autom.*, 2010, pp. 2529–2536.

Curvature-Bounded Traversability Analysis in Motion Planning for Mobile Robots

Raghvendra V. Cowlagi and Panagiotis Tsiotras

Abstract—We consider the geometric problem of deciding whether a narrow planar passage can be traversed by a curve that satisfies prespecified upper bounds on its curvature. This problem is of importance for path- and motion-planning of autonomous mobile robots, particularly when vehicle dynamical constraints are considered during planning. For a special case of narrow passages, namely, rectangular channels, we present a fast numerical algorithm to determine if a given channel may be traversed via curvature-bounded paths. We demonstrate that the proposed algorithm can affirm traversability in cases where the most recent result in the literature fails.

Index Terms—Mobile robots, motion planning, robot kinematics.

I. INTRODUCTION

CONSIDER the following problem in planar geometry: Let \mathcal{P} be a polygon, with two of its edges designated as the *entry* and *exit* edges. Determine if there exists a continuously differentiable curve of finite length and with no cusps, such that this curve lies entirely within the polygon \mathcal{P} , the endpoints of this curve lie on the entry and exit edges, and the curvature of this curve satisfies, pointwise, a prespecified upper bound. The bound on the curvature may vary over the region enclosed by \mathcal{P} .

Manuscript received November 15, 2013; revised January 30, 2014; accepted March 31, 2014. Date of publication April 24, 2014; date of current version August 4, 2014. This paper was recommended for publication by Associate Editor S. Carpin and Editor C. Torras upon evaluation of the reviewers' comments. This work was supported in part by the Army Research Office Multidisciplinary University Research Initiative Award #W911NF-11-1-0046.

R. V. Cowlagi is with the Aerospace Engineering Program, Worcester Polytechnic Institute, Worcester, MA 01609 USA (e-mail: rvowlagi@wpi.edu). P. Tsiotras is with the School of Aerospace Engineering, Georgia Institute of Technology, Atlanta, GA 30332 USA (e-mail: tsiotras@gatech.edu).

Color versions of one or more of the figures in this paper are available online at <http://ieeexplore.ieee.org>.

Digital Object Identifier 10.1109/TRO.2014.2315711

Problems of this nature may be called *traversability analysis* problems to distinguish them from path- and motion-planning problems [1] and are frequently encountered in mobile robotics applications. Whereas the former class of problems emphasizes the *existence* of a curve with special geometric characteristics, the latter class of problems emphasizes the *construction* thereof. In this paper, we discuss the solution of a special case of a *curvature-bounded traversability analysis* (CBTA) problem, and we highlight the role of CBTA problems in motion planning for mobile robots.

A. Related Work

A fundamental result on CBTA is that the following problem is *decidable* [2]: Given a polygon, find a curve that connects two prespecified configurations (position and orientation), such that it lies entirely within the given polygon, and satisfies a unit curvature bound. A decision procedure provided in [2] solves a special CBTA problem; namely, the case of a uniform curvature bound and with prespecified initial and final configurations. Note that if the CBTA of interest does not include a specific initial or final configuration, then the decision procedure of [2] is not directly applicable. In this context, the analysis of the reachability of points within a polygon by curvature-bounded paths [3] is more relevant.

In [4], CBTA of a polygon is discussed in the context of existence of curvature-bounded paths in a neighborhood of a prespecified path that traverses the polygon. This neighborhood is called a *channel*, and it is the union of the family of discs of a constant radius w , with centers along the prespecified path. The main result of [4] states that unit curvature-bounded traversal of a channel is guaranteed if $w \geq \tau$, where $\tau \approx 1.55$. This condition is sufficient for traversability, but it is not necessary; we provide an example where this condition is violated, yet curvature-bounded traversal is possible, and established by the proposed approach.

The literature on curvature-bounded path planning is significantly wider than that on CBTA because *the existence of such a path is assumed*. In the absence of obstacles, the shortest curvature-bounded path between two prespecified configurations was shown to lie in a finite family of paths (henceforth referred to as *Dubins paths*), first via geometric arguments [5] and later via optimal control theory [6]. In the presence of polygonal obstacles, the problem of finding a shortest curvature-bounded path between two prespecified configurations was shown to be NP-hard [7]. Algorithms for approximating the shortest path in the presence of obstacles appear, for example, in [8]–[11]. Path planning under the additional restriction of *continuity* in the curvature of paths is discussed in [12]–[14].

B. Contributions

In this paper, we precisely state and solve the following CBTA problem: Decide whether a *rectangular channel* can be traversed by a curve that satisfies pre-specified upper bounds on its curvature. A rectangular channel is a passage formed by a sequence of rectangles with disjoint interiors. The main contributions of this paper are as follows.

First, we propose a computationally fast technique to solve the CBTA problem for the case of rectangular channels, which has been of great research interest in the field of computational geometry [4]. Moreover, a conservative solution to the CBTA of a general polygonal region can be found by internally approximating the polygon by a rectangular channel. The proposed technique does not require specific initial and final configurations, and hence, it is applicable in cases where the approach of [2] is not. Stated differently, the proposed techniques achieve, via discretization of one variable (namely, initial position), traversability

results that the approach of [2] would achieve via discretization over *four* variables (namely, initial and final positions and initial and final orientations).

Similarly, the proposed technique is capable of performing CBTA in cases where the most recent result in the literature [4] fails to provide any useful information. Furthermore, the proposed technique allows *nonuniform channel width*, which is not addressed in [4], and it also allows *nonuniform curvature constraints*, which are not addressed in any of the CBTA-related papers [2]–[4], or in any of the path-planning-related papers [8]–[11].

Second, we discuss the fundamental role and application of CBTA to the problem of motion planning for autonomous mobile vehicles. Real-time motion planning in the presence of complex vehicle dynamical constraints is a problem of active research, and the use of geometric methods is considered critical for computational efficiency [15]. In this paper, we discuss how CBTA problems arise naturally in motion planning from the geometric traversal constraints imposed by the vehicle dynamic constraints. We demonstrate how a CBTA-based technique can be used to transform these constraints to *convex* constraints to enable real-time implementation.

Finally, we discuss other robotics-related applications of CBTA (see Section I-C), thus contributing to the practical use of ideas and results from computational geometry for research and development in robotics and autonomous systems.

Preliminary versions of the discussion and results presented in this paper were previously presented in [16]. This paper presents detailed algorithms for the solution of the CBTA problem, a complete proof of Theorem 1, and applications of the proposed technique, neither of which appeared in [16].

C. Applications of Curvature-Bounded Traversability Analysis

For motion planning of autonomous mobile vehicles, CBTA is important because the curvatures of planar geometric paths that a vehicle can feasibly traverse are upper-bounded. The curvature of the path traversed by a vehicle is $\kappa = |\dot{\theta}/v|$, where v is the speed, and θ is the direction (heading) of the velocity vector of the vehicle. Bounds on this curvature stem from 1) nonholonomic kinematic constraints in conjunction with bounds on velocity variables and 2) acceleration constraints that result from limited force and torque inputs to the vehicle. An example of the former category is the Dubins car [6], which is a model of a vehicle that moves forward with constant speed and bounded turn rate. Examples of the latter category are the aircraft navigational model [17] with bounded load factor, and the half-car dynamical model [18] with bounded magnitude of ground-tire friction forces at each tire. These constraints on the tire friction forces are shown in [19] to be equivalent to a state-dependent curvature bound on the motion of a point, called the center of oscillation, associated with the half-car.

Optimal path- and motion-planning for vehicles with such kinematic and dynamic constraints is difficult, yet crucial, for vehicle autonomy. Recently, we developed an optimal motion planner for such vehicles [15]. This motion planner is based upon two key ideas: 1) rectangular *multiresolution cell decompositions* that represent the environment map with a graph and allow the use of fast path optimization techniques for graphs and 2) *history-dependent* transition costs in the cell decomposition graph that allow the incorporation of vehicle kinematic and dynamic constraints. As discussed in detail in [15], a subproblem that is repeatedly encountered and solved in this motion planner is that of analyzing the feasibility of the traversal of a “channel” defined by a sequence of successively adjacent rectangular cells, and then of finding a specific motion that enables this traversal.

Whereas real-world features are approximated by rectangular cell decompositions, path-planning algorithms based on such decompositions exhibit the property of *resolution completeness* [1]. This property implies that the path-planning algorithm is guaranteed to find a path, if it exists, in the limit as cell size approaches zero. Therefore, this property provides a sound basis for using rectangular cell decompositions in path planning and, consequently, reinforces the importance of the proposed CBTA of rectangular channels.

Because of the aforesaid relation between bounds on the curvatures of feasible paths that arise due to the vehicle's kinematical and dynamical constraints, the analysis of feasibility of traversal across such "channels" is a CBTA problem. In addition to establishing feasibility of traversal, the results of this CBTA can also be applied to simplify the search for a specific motion that enables this traversal [20].

In general, CBTA finds applications to problems in mobile robotics whenever it is convenient and/or necessary to identify a region of feasible traversal. In the context of curvature-bounded traversal of polygonal regions with polygonal obstacles, it is computationally efficient to find a path consisting of straight line segments with a guaranteed "clearance" distance from all obstacle boundaries [4]. Similarly, for semiautonomous high-speed driving, the identification of a homotopic class of curvature-bounded paths is discussed in [21]. The main idea in [21] is to assist human drivers of ground vehicles by finding a region that is guaranteed to be both safe and feasible for traversal. The approach considered in [21] for finding this homotopic class is heuristic, and a rigorous approach for the same application may be developed using CBTA. Finally, CBTA may be applied to motion planning for highly flexible robotic manipulators such as flexible medical needles and catheters: Curvature-bounded path planning for such manipulators has been considered, for instance, in [22], where the need for computing paths with maximal clearance from obstacles—and, consequently, the problem of identifying safe passages for the manipulator—has been emphasized.

The rest of this paper is organized as follows. In Section II, we define the CBTA problem of interest and outline the proposed numerical algorithm for its solution. In Section III, we provide examples that illustrate the benefits of the proposed technique over existing results in the literature and its applications to motion planning for mobile robots. We conclude the paper in Section IV with comments on future work.

II. TRAVERSABILITY ANALYSIS

To fix ideas, we first establish some terminology. A *path between two points* P and Q in the plane is a differentiable curve $\Gamma := \{s \mapsto [x(s), y(s)] \in \mathbb{R}^2 : 0 \leq s \leq 1\}$ such that $P = [x(0), y(0)]$ and $Q = [x(1), y(1)]$. We will denote by $\Gamma(s)$ the point $[x(s), y(s)] \in \mathbb{R}^2$ on the path Γ , and by $\Gamma'(W)$ the angle of the tangent to Γ at the point $W = [x(s), y(s)]$ for all $s \in [0, 1]$. In addition, we will denote by (W, α) the configuration in \mathcal{C} specified by the position $W \in \mathbb{R}^2$ and the orientation $\alpha \in [-\pi, \pi]$. A *path between a configuration* (W, α) and a point X is a path Γ between the points W and X satisfying $\Gamma'(W) = \alpha$. Similarly, a *path between two configurations* (W, α) and (X, β) is a path Γ between the points W and X satisfying $\Gamma'(W) = \alpha$ and $\Gamma'(X) = \beta$.

Definition 1: A rectangular channel $\bar{\mathcal{R}}^C$ is a sequence of rectangles $\{R_n\}_{n=1}^C$, $C \in \mathbb{N}$, with disjoint interiors, such that we have the following.

- 1) Exactly one edge of R_n has a nonempty intersection with exactly one edge of R_{n+1} for each $n \in \{1, \dots, C-1\}$.
- 2) For all $m, n \in \{1, \dots, C\}$, the edges of R_n and R_m do not intersect or overlap whenever $m \notin \{n-1, n, n+1\}$.

Next, we precisely define the CBTA problem for a rectangular channel, which is a simplification of the general problem introduced in

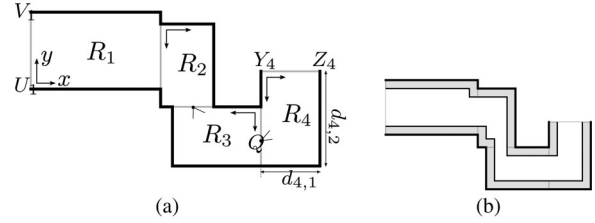


Fig. 1. Rectangular channels. (a) Example of a rectangular channel. (b) Channel obtained by shrinking the boundaries of a rectangular channel.

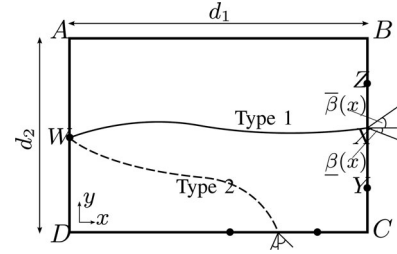


Fig. 2. Type 1 and Type 2 paths.

Section I. Rectangular channels [see Fig. 1(a)] naturally arise from rectangular cell decompositions. Furthermore, the polygon obtained by shrinking the boundaries of a rectangular channel [see Fig. 1(b)] is also a rectangular channel. Therefore, the proposed CBTA technique can be applied *with no modifications* to the new channel. The proposed CBTA technique may, thus, be used in motion-planning algorithms that also incorporate the shape of a mobile vehicle. Note that this approach of shrinking channels has limitations for oblong or other irregular shapes. **CBTA-R Problem:** Let $\bar{\mathcal{R}}^C$ be a rectangular channel, and let W be a point on any one of the three edges of R_1 that do not intersect R_2 . Let $\alpha \in [-\pi, \pi]$ be a specified angle. For any set of positive real numbers $r_n > 0$, $n = 1, \dots, C$, determine if there exists a path Γ such that we have the following.

- 1) $\Gamma(0) = W$, and $\Gamma'(W) = \alpha$.
- 2) The point $X := \Gamma(1)$ lies on an edge of the rectangle R_C (pre-specified from among the three edges of R_C that do not overlap with any edge of R_{C-1}), and $\Gamma'(X)$ lies in a specified set of allowable terminal tangent angles.
- 3) The path Γ does not leave $\bar{\mathcal{R}}^C$, i.e., $(x(s), y(s)) \in \cup_{n=1}^C R_n$ for all $s \in [0, 1]$.
- 4) For each $n = 1, \dots, C$, the curvature of Γ at any point within the rectangle R_n is at most r_n^{-1} .

In what follows, we will refer to any path Γ that satisfies the conditions of CBTA-R as an *admissible* path. We propose a numerical algorithm to solve CBTA-R that is based on a recursive CBTA of the individual rectangles within the rectangular channel. Specifically, the proposed algorithm is based on recursive backward propagation of so-called *target configuration sets*. Informally, these sets are intervals of allowable orientations associated with all points on the segments defined by $R_n \cap R_{n+1}$, $n \in \{1, \dots, C-1\}$. Next, we provide a precise description of these sets.

Let $ABCD$ be a rectangle. We attach a Cartesian axes system as shown in Fig. 2. Let the dimensions of the rectangle be d_1 and d_2 , and let $r > 0$ be fixed.

Definition 2: Let $\underline{\beta}(x), \bar{\beta}(x)$, $x \in [0, d_2]$ be functions such that $-\frac{\pi}{2} \leq \underline{\beta}(x) \leq \bar{\beta}(x) \leq \frac{\pi}{2}$. Let $Y = (d_1, y)$, $Z = (d_1, z)$ be points on

the segment BC with $y \leq z$. A path Γ whose endpoints lie on the segments DA and YZ , respectively, is a Type 1 path if it satisfies the following.

- 1) (Curvature Boundedness): The curvature at any point on Γ is at most r^{-1} .
- 2) (Containment): All points of Γ lie in the closed interior of the rectangle $ABCD$.
- 3) (Terminal Orientation): $\Gamma'(X) \in [\underline{\beta}(x), \overline{\beta}(x)]$.

A Type 2 path is defined analogously for traversal across adjacent edges (see Fig. 2).

Definition 3: Let $\underline{\beta}(x), \overline{\beta}(x)$, $x \in [0, d_1]$ be functions, such that $-\frac{\pi}{2} \leq \underline{\beta}(x) \leq \overline{\beta}(x) \leq \frac{\pi}{2}$. Let $Y = (y, 0)$, $Z = (z, 0)$ be points on the segment DC with $y \leq z$. A path Γ whose endpoints lie on the segments DA and YZ , respectively, is a Type 2 path if it satisfies the following.

- 1) The curvature at any point on Γ is at most r^{-1} .
- 2) All points of Γ lie in the closed interior of the rectangle $ABCD$.
- 3) $\Gamma'(X) + \frac{\pi}{2} \in [\underline{\beta}(x), \overline{\beta}(x)]$.

Based on these definitions, we specify two CBTA problems for a rectangle that will be solved repeatedly for the CBTA of the overall rectangular channel. Let $\underline{\beta}, \overline{\beta}, Y$, and Z be as in the preceding definitions. Let $W = (0, w)$ and $r > 0$ be fixed.

CBTA-S1 Problem: Find $\underline{\alpha}, \overline{\alpha}$ such that for every $\alpha \in [\underline{\alpha}, \overline{\alpha}]$, there exists a Type 1 path Γ with $\Gamma(0) = W$ and $\Gamma'(W) = \alpha$.

CBTA-S2 Problem: Find $\underline{\alpha}, \overline{\alpha}$ such that for every $\alpha \in [\underline{\alpha}, \overline{\alpha}]$, there exists a Type 2 path Γ with $\Gamma(0) = W$ and $\Gamma'(W) = \alpha$.

We describe next a recursive procedure to solve CBTA-R.

A. Recursive Constructions of Target Configuration Sets

We attach a coordinate axes system to each rectangle of $\overline{\mathcal{R}}^C$ in a manner consistent with the axes system used in the statement of CBTA-S1 and CBTA-S2 [see Fig. 1(a)]. Let the dimensions of each rectangle along the x and y axes be denoted, respectively, by $d_{n,1}$ and $d_{n,2}$. We may identify rigid geometric transformations (i.e., a sequence of rotations and reflections) that align the entry and exit segments of R_n to the segments AD and BC , respectively, for traversal across parallel edges, or to the segments AD and DC , respectively, for traversal across adjacent edges. Let ϱ_n denote the minimum number of reflections involved in the transformation associated with the rectangle R_n .

For each rectangle R_n , $n = 2, 3, \dots, C-1$, we refer to the segments formed by the intersections $R_{n-1} \cap R_n$ and $R_n \cap R_{n+1}$, respectively, as the *entry and exit segments*, and we denote by U_n and V_n (respectively, Y_n, Z_n) the endpoints of the entry (respectively, exit) segment. Finally, we denote the coordinates of the points U_n, V_n, Y_n, Z_n , by the corresponding lower case letters, i.e., $V_n = (0, v_n)$, etc.

As previously noted, the algorithm to solve CBTA-R involves the recursive backward propagation of target configuration sets. For every point $Q = (q, 0)$ [or $Q = (d_{n,1}, q)$, as applicable], on the segment $Y_n Z_n$, $n = 1, \dots, C$, we denote by $\underline{\beta}_n(q)$ and $\overline{\beta}_n(q)$, respectively, the lower and upper bounds of the allowable terminal orientations for $q \in [y_n, z_n]$. Similarly, for every point $P = (0, p)$ on the segment $U_n V_n$, $n = 1, \dots, C$, we denote by $\underline{\alpha}_n(p)$ and $\overline{\alpha}_n(p)$, respectively, the lower and upper bounds resulting from the solution of CBTA-S1 (or CBTA-S2, as applicable), for $p \in [u_n, v_n]$. Note that $[\underline{\alpha}_n(p), \overline{\alpha}_n(p)]$ is the interval of allowable orientations at point P in the effective target configuration set of the rectangle R_{n-1} . The angles $\underline{\alpha}_n(\cdot), \overline{\alpha}_n(\cdot), \underline{\beta}_n(\cdot)$, and $\overline{\beta}_n(\cdot)$ are measured in the coordinate axes system attached to R_n .

The recursive algorithm for constructing the effective target configuration sets is provided in Fig. 3. Next, we focus on the solutions of CBTA-S1 and CBTA-S2.

Traversability Analysis of Rectangular Channels

Input: $\overline{\mathcal{R}}^C$, **Output:** $\underline{\alpha}_n, \overline{\alpha}_n$, for each $n \in \{1, \dots, C\}$

- 1: $\overline{\alpha}_{C+1}(q) \leftarrow \frac{\pi}{2}$ and $\underline{\alpha}_{C+1}(q) \leftarrow -\frac{\pi}{2}$,
for all $q \in [0, d_{C,2}]$ if R_C involves traversal across parallel edges, or otherwise,
for all $q \in [0, d_{C,1}]$ if R_C involves traversal across adjacent edges.
- 2: $\varrho_{C+1} \leftarrow 0$
- 3: **for** $n = C, C-1, \dots, 1$ **do**
- 4: **if** $\varrho_n + \varrho_{n-1}$ is odd **then**
- 5: $\underline{\beta}_n(q) \leftarrow -\overline{\alpha}_{n+1}(y_n - (p - v_{n+1}))$, for
 $p \in [u_{n+1}, v_{n+1}]$, $q \in [y_n, z_n]$
- 6: $\overline{\beta}_n(q) \leftarrow -\underline{\alpha}_{n+1}(y_n - (p - v_{n+1}))$, for
 $p \in [u_{n+1}, v_{n+1}]$, $q \in [y_n, z_n]$
- 7: **else**
- 8: $\underline{\beta}_n(q) \leftarrow \underline{\alpha}_{n+1}(p)$, for $p \in [u_{n+1}, v_{n+1}]$, $q \in [y_n, z_n]$
- 9: $\overline{\beta}_n(q) \leftarrow \overline{\alpha}_{n+1}(p)$, for $p \in [u_{n+1}, v_{n+1}]$, $q \in [y_n, z_n]$
- 10: **Find** $\underline{\alpha}_n(q)$ and $\overline{\alpha}_n(q)$ for $q \in [u_n, v_n]$ by CBTA-S1 or CBTA-S2 for rectangle R_{n-1} .

Fig. 3. Pseudocode of the recursive procedure to solve CBTA-R via computations of effective target configuration sets.

B. Curvature-Bounded Traversability Analysis of a Single Rectangle

CBTA-S1 (respectively, CBTA-S2) involves finding $\underline{\alpha}$ and $\overline{\alpha}$ such that, if $\alpha \in [\underline{\alpha}, \overline{\alpha}]$, then there exists a Type 1 (respectively, Type 2) path Γ with $\Gamma(0) = W$ and $\Gamma'(W) = \alpha$. To solve CBTA-S1, we construct families of Type 1 paths Υ_x and Λ_x between the points W and X , for every point $X = (d_1, x)$ on the segment YZ , satisfying the following properties:

- P1) $\Lambda'_x(W) \leq \Upsilon'_x(W)$.
- P2) For every $\alpha \in [\Lambda'_x(W), \Upsilon'_x(W)]$, there exists a Type 1 path from W to X with tangent angle α at W .
- P3) The angles $\Upsilon'_x(W)$ and $\Lambda'_x(W)$ vary continuously with x .
- P4) There exists no other Type 1 path Γ from W to X satisfying P1)–P3) such that $\Gamma'(W) > \Upsilon'_x(W)$.
- P5) There exists no other Type 1 path Γ from W to X which satisfies P1)–P3) such that $\Gamma'(W) < \Lambda'_x(W)$.

We may define analogous properties for Type 2 paths to solve CBTA-S2. The following result enables the solutions to CBTA-S1 and CBTA-S2 based on the paths Υ_x and Λ_x . The constructions of Υ_x and Λ_x are implicit in the calculations of the angles $\underline{\alpha}$ and $\overline{\alpha}$. Properties P1)–P5) are not assumed *a priori*; rather, Υ_x and Λ_x are constructed such that these properties can be proven. Examples of the constructions of Υ_x and Λ_x are provided in the Appendix, whereas the (laborious and geometrically involved) proofs that these constructions satisfy the properties P1)–P5) are available in [17].

Theorem 1: Suppose there exists a closed interval $\mathcal{I} \subset [y, z]$ such that Type 1 (respectively, Type 2) paths Υ_x and Λ_x satisfying P1)–P5) exist for each $x \in \mathcal{I}$. Then, $\overline{\alpha}$ and $\underline{\alpha}$ defined by

$$\underline{\alpha} := \min_{x \in \mathcal{I}} \{\Lambda'_x(W)\}, \quad \overline{\alpha} := \max_{x \in \mathcal{I}} \{\Upsilon'_x(W)\}, \quad (1)$$

solve CBTA-S1 (respectively, CBTA-S2).

Proof: The numbers $\underline{\alpha}$ and $\overline{\alpha}$ are well defined by (1) because \mathcal{I} is closed and bounded, and because $\Lambda'_x(W), \Upsilon'_x(W)$ are continuous in x by (P3). We claim that for every $\alpha \in [\underline{\alpha}, \overline{\alpha}]$, there exists $x_\alpha \in \mathcal{I}$ such

that $\alpha \in [\underline{\Lambda}'_{x_\alpha}(W), \Upsilon'_{x_\alpha}(W)]$. To see this, suppose, for the sake of contradiction, that no such x_α exists. Then, by P1), for every $x \in \mathcal{I}$, exactly one of the following conditions must hold true:

$$\alpha < \Lambda'_x(W) \leq \Upsilon'_x(W) \quad (2a)$$

$$\alpha > \Upsilon'_x(W) \geq \Lambda'_x(W). \quad (2b)$$

Because $\alpha \in [\underline{\alpha}, \bar{\alpha}]$, by (1), neither (2a) nor (2b) can exclusively hold true for all $x \in \mathcal{I}$. Consequently, there exists $\tilde{x} \in \mathcal{I}$ such that condition (2a) switches at \tilde{x} from being true to being false or *vice versa*. By continuity of $\Lambda'_x(W)$ in x , it follows that $\alpha = \Lambda'_{\tilde{x}}(W) \leq \Upsilon'_{\tilde{x}}(W)$. Thus, for \tilde{x} , condition (2a) does not hold true, which implies that (2b) must hold true, which in turn implies that $\alpha > \Upsilon'_{\tilde{x}}(W)$. Thus, we reach a contradiction, which implies that there exists $x_\alpha \in \mathcal{I}$, as previously stated. It follows by P2) that there exists a Type 1 path (respectively, Type 2 path) Γ between W and $X = (d_1, x_\alpha)$ such that $\Gamma'(W) = \alpha$, and thus, $\underline{\alpha}$ and $\bar{\alpha}$ solve CBTA-S1 (respectively, CBTA-S2). ■

By Theorem 1, the solutions to CBTA-S1 and CBTA-S2 may be found by 1) constructing the families of paths Υ_x and Λ_x that satisfy the properties¹ P1)–P5) and 2) computing the angles $\Upsilon'_x(W)$ and $\Lambda'_x(W)$ and their maximum and minimum values, respectively, for $x \in \mathcal{I}$.

We will postpone the description of the geometric details of the constructions of the paths Υ_x and Λ_x to the Appendix, and instead, we will focus here on the computations of the tangent angles $\Upsilon'_x(W)$ and $\Lambda'_x(W)$. For the sake of clarity of exposition, we will assume in the rest of this paper that $r > d := d_1$ and that $d_1 = d_2$. Note that the overall approach, as hitherto described, remains the same when these assumptions are removed. The complete details of the constructions of Υ_x and Λ_x and the computations of $\Upsilon'_x(W)$ and $\Lambda'_x(W)$ without these assumptions are available in [17, ch. 5 and App. C].

Fig. 4 shows the procedure for computing $\Upsilon'_x(W)$ for the problem of traversal across parallel edges (CBTA-S1), Fig. 5 shows the procedure for $\Upsilon'_x(W)$ for traversal across adjacent edges (CBTA-S2), and Fig. 6 shows the procedure for computing $\Lambda'_x(W)$ for (CBTA-S2). Note that the computation of $\Lambda'_x(W)$ for CBTA-S1 may be performed using the procedure shown in Fig. 4 by replacing w with $d - w$, $\underline{\beta}(x)$ with $-\underline{\beta}(d - x)$, $\bar{\beta}(x)$ with $-\bar{\beta}(d - x)$, and by reversing the sign of the result. The following notation is used in Figs. 4–6:

$$\begin{aligned} \sigma_1 &:= r \cos \underline{\beta}(x) + (x - w), & \sigma_4 &:= r \sin \underline{\beta}(x) - w \\ \sigma_2 &:= r \sin \underline{\beta}(x) - d, & \sigma_5 &:= -r \cos \underline{\beta}(x) - x \\ \sigma_3 &:= (d^2 + (x - w)^2)/2r, & \sigma_6 &:= (w^2 + x^2)/2r. \end{aligned}$$

To summarize, we solve CBTA-R by recursively solving two simpler CBTA problems, denoted by CBTA-S1 and CBTA-S2, which are defined over a single rectangle. Next, we solve CBTA-S1 and CBTA-S2 by constructing families of special geometric paths that satisfy properties P1)–P5), followed by the application of Theorem 1.

C. Illustrative Example

To illustrate the solution of CBTA-S1 given by the procedure in Fig. 4, we consider a square of size $d = 10$ and $r = 45$. We assume that the exit segment YZ is such that the point Y coincides with the point C (i.e., $y = 0$) and that the point Z coincides with the midpoint of the segment BC (i.e., $z = 5$), as shown in Fig. 7. For simplicity, we

¹Note that properties P4) and P5) are not required to prove Theorem 1; they ensure that the solutions to CBTA-S1 and CBTA-S2 are not conservative.

Computation of $\Upsilon'_x(W)$ for CBTA-S1

- 1: $\alpha^*(w) \leftarrow \cos^{-1}(1 - (d - w)/r)$
- 2: **if** $2r(d - w) < d^2 + (d - w)^2$ **then**
- 3: $n_2 \leftarrow w + \sqrt{r^2 - (r \sin(\alpha^*(w)) - d)^2} - r \cos(\alpha^*(w))$
- 4: **else**
- 5: $n_2 \leftarrow d$
- 6: For $x \in [y, n_2] \cap [y, z]$, find $\gamma^*(x) \in [-\frac{\pi}{2}, \frac{\pi}{2}]$ by solving
$$(x - w) \cos(\gamma^*(x)) - d \sin(\gamma^*(x)) = \sigma_3. \quad (3)$$
- 7: **if** $\gamma^*(x) < \underline{\beta}(x)$ **then**
- 8: Find $\Upsilon'_x(W) \in [-\frac{\pi}{2}, \frac{\pi}{2}]$ by solving
$$\sigma_1 \cos(\Upsilon'_x(W)) + \sigma_2 \sin(\Upsilon'_x(W)) + (x - w) \cos \underline{\beta}(x) - d \sin \underline{\beta}(x) + \sigma_3 = 1. \quad (4)$$
- 9: **if** $\underline{\beta}(x) \leq \gamma^*(x) < \bar{\beta}(x)$ **then**
- 10: Find $\Upsilon'_x(W) \in [-\frac{\pi}{2}, \frac{\pi}{2}]$ by solving
$$-(x - w) \cos(\Upsilon'_x(W)) + d \sin(\Upsilon'_x(W)) = \sigma_3. \quad (5)$$
- 11: **if** $\bar{\beta}(x) < \gamma^*(x)$ **then**
- 12: Υ_x does not exist

Fig. 4. Computation of $\Upsilon'_x(W)$ for CBTA-S1.

Computation of $\Upsilon'_x(W)$ for CBTA-S2

- 1: For all $x \in [y, z]$, find $\gamma^*(x) \in [-\frac{\pi}{2}, \frac{\pi}{2}]$ by solving
$$x \cos(\gamma^*(x)) - w \sin(\gamma^*(x)) = \sigma_6.$$
- 2: **if** $\gamma^*(x) < \underline{\beta}(x)$ **then**
- 3: Find $\Upsilon'_x(W) \in [-\frac{\pi}{2}, \frac{\pi}{2}]$ by solving
$$\sigma_4 \cos(\Upsilon'_x(W)) + \sigma_5 \sin(\Upsilon'_x(W)) + x \cos \underline{\beta}(x) - w \sin \underline{\beta}(x) + \sigma_6 = 1.$$
- 4: **if** $\underline{\beta}(x) \leq \gamma^*(x) < \bar{\beta}(x)$ **then**
- 5: Find $\Upsilon'_x(W) \in [-\frac{\pi}{2}, \frac{\pi}{2}]$ by solving
$$w \cos(\gamma^*(x)) + x \sin(\gamma^*(x)) = \sigma_6.$$
- 6: **if** $\bar{\beta}(x) < \gamma^*(x)$ **then**
- 7: Υ_x does not exist

Fig. 5. Computation of $\Upsilon'_x(W)$ for CBTA-S2.

assume that the terminal orientation constraints, i.e., the maps $\underline{\beta}$ and $\bar{\beta}$ have the constant values of $\underline{\beta}(x) = -40^\circ$ and $\bar{\beta}(x) = 10^\circ$ for all $x \in [y, z]$. These constraints are indicated by the red and blue arrows on segment YZ in Fig. 7.

Next, we execute the procedure in Fig. 4 repeatedly, for several values of $w \in [0, d]$. These values may be chosen, for example, by uniform discretization of the interval $[0, d]$. In the numerical calculations for this example and for Example 1 in Section III, we used a uniform discretization with 20 points. Note that a discretization with

Computation of $\Lambda'_x(W)$ for CBTA-S2

- 1: $n_1 \leftarrow r - \sqrt{r^2 - w^2}$
- 2: For all $x \in [n_1, z]$, find $\gamma^*(x) \in [-\frac{\pi}{2}, \frac{\pi}{2}]$, by solving

$$-x \cos(\gamma^*(x)) + w \sin(\gamma^*(x)) = \sigma_6.$$
- 3: **if** $\bar{\beta}(x) < \gamma^*(x)$ **then**
- 4: Find $\Lambda'_x(W) \in [-\frac{\pi}{2}, \frac{\pi}{2}]$ by solving

$$\sigma_7 \cos(\Lambda'_x(W)) + \sigma_8 \sin(\Lambda'_x(W)) + x \cos \underline{\beta}(x) - w \sin \underline{\beta}(x) + \sigma_6 = 1.$$
- 5: **if** $\underline{\beta}(x) \leq \gamma^*(x) < \bar{\beta}(x)$ **then**
- 6: Find $\Lambda'_x(W) \in [-\frac{\pi}{2}, \frac{\pi}{2}]$ by solving

$$-w \cos(\gamma^*(x)) - x \sin(\gamma^*(x)) = \sigma_6.$$
- 7: **if** $\gamma^*(x) < \underline{\beta}(x)$ **then**
- 8: Λ_x does not exist

Fig. 6. Computation of $\Lambda'_x(W)$ for CBTA-S2.

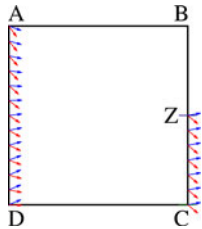


Fig. 7. Example of the solution of CBTA-S1.

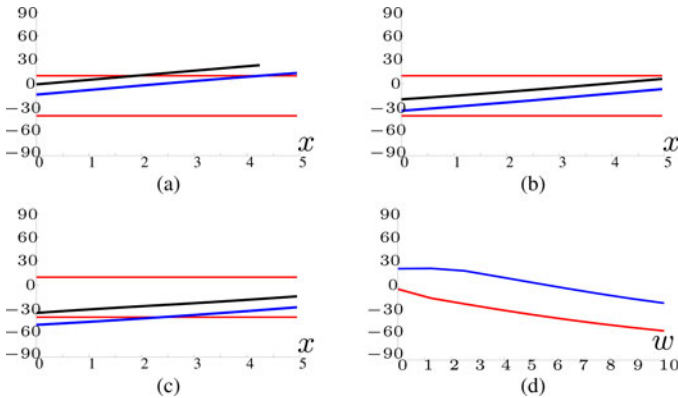


Fig. 8. Intermediate calculations in the procedure shown in Fig. 4.

sufficiently high resolution is required for the correct determination of traversability of a given channel.

For illustrative purposes, suppose $w = 5$. By line 1 in Fig. 4, we compute $\alpha^*(w) = 27.26^\circ$. Next, by line 2, we observe that $2r(d - w) < d^2 + (d - w)^2$, and hence, $n_2 = d = 10$. Next, by line 6, we solve (3) for several values of $x \in [0, 5]$. In the numerical calculations for this example and for Example 1 in Section III, we used a uniform discretization with 20 points. The values taken by $\gamma^*(x)$ for $w = 5$ are indicated by the blue-colored curve in Fig. 8(b). In Fig. 8(b), the red-colored curves indicate, respectively, the (constant) values taken by $\underline{\beta}(x)$ and $\bar{\beta}(x)$. We observe that $\underline{\beta}(x) < \gamma^*(x) < \bar{\beta}(x)$ for every

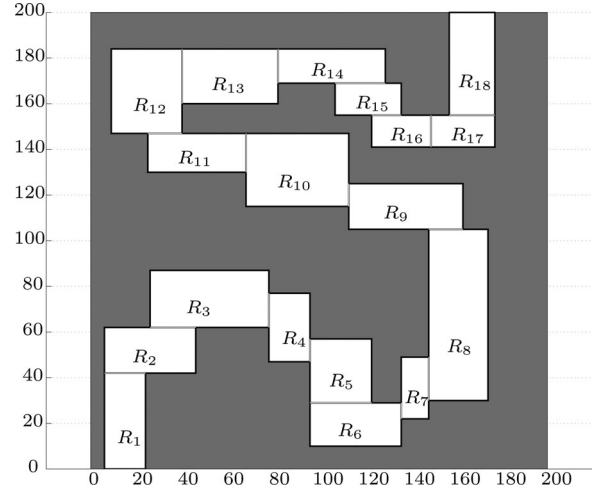


Fig. 9. Example of a rectangular channel for which the result of [4] fails.

TABLE I
SIZES OF RECTANGLES AND CURVATURE CONSTRAINTS FOR EXAMPLE 1

	Size	r		Size	r		Size	r
R_1	42×18	15	R_2	20×40	15	R_3	25×52	12
R_4	18×30	12	R_5	27×28	14	R_6	19×40	14
R_7	12×27	16	R_8	26×75	25	R_9	20×50	22
R_{10}	45×32	20	R_{11}	43×17	13	R_{12}	37×31	16
R_{13}	42×24	18	R_{14}	47×15	20	R_{15}	14×29	20
R_{16}	14×26	19	R_{17}	28×14	15	R_{18}	45×20	18

$x \in [y, z]$. Hence, by lines 9 and 10, we compute $\Upsilon'_x(W)$ by solving (5), which is indicated by the black-colored curve in Fig. 8(b). The values taken by $\gamma^*(x)$ and $\Upsilon'_x(W)$ for $w = 1.25$ and $w = 8.75$ are indicated in Figs. 8(a) and (c), respectively.

As previously noted, this procedure may be used to compute $\Lambda'_x(w)$ by replacing w with $d - w$, $\underline{\beta}(x)$ with $-\bar{\beta}(d - x)$, $\bar{\beta}(x)$ with $-\underline{\beta}(d - x)$, and by reversing the sign of the result. The values of $\underline{\alpha}$ and $\bar{\alpha}$ for all values of $w \in [0, d]$, computed using (1), are indicated, respectively, in Fig. 8(d) by the red- and blue-colored curves.

The trigonometric equations (3)–(5) can be easily transformed to quadratic equations in a new variable. Consequently, the solutions of these equations are computationally fast: For example, the MATLAB-based computation of $\underline{\alpha}$ and $\bar{\alpha}$ for 100 different values of $w \in [0, d]$ was performed in 60 ms on a computer with an Intel Core i7-2640M processor, operating at 2.80 GHz with 8 GB of memory. These computations will be significantly quicker when computations are performed using a lower-level programming language such as C or C++.

III. CURVATURE-BOUNDED TRAVERSABILITY ANALYSIS APPLICATIONS

In this section, we demonstrate the benefits of the proposed CBTA technique with 1) an example that demonstrates the benefits of the proposed technique over existing results in the literature and 2) an example of the application of CBTA to robot motion planning via model predictive control (MPC).

Example 1: To illustrate the benefits of the proposed technique over existing results in the literature, we consider the CBTA of the rectangular channel shown in Fig. 9. The dimensions of each of the rectangles and the specified minimum radii of turn r^{-1} in general units (inverse of maximum curvature) within each rectangle are provided in Table I. We apply the CBTA procedure given in Fig. 3. In this recursive procedure,

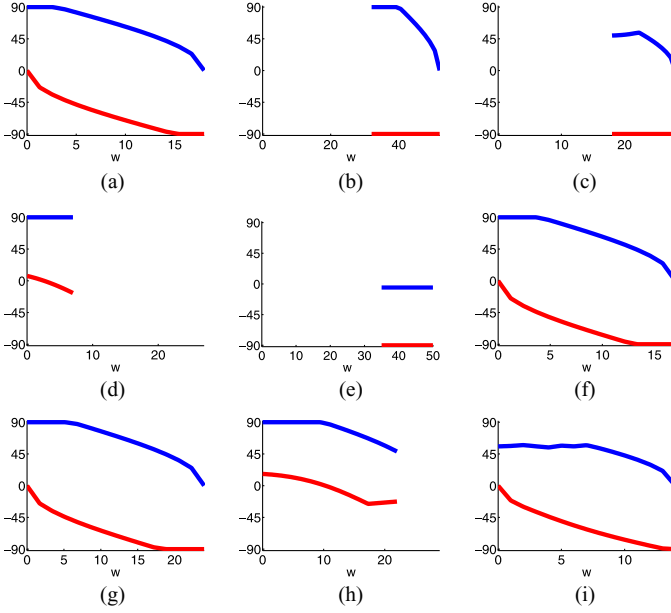


Fig. 10. Target configuration sets for rectangles in the channel in Fig. 9.

we solve CBTA-S1 and CBTA-S2, as applicable, for each rectangle using general versions of the procedures given in Figs. 4–6 (see [17], App. C) for details).

The values taken by $\underline{\alpha}_n$ and $\bar{\alpha}_n$, for some values of $n \in \{1, \dots, 18\}$, are indicated, respectively, by the red- and blue-colored curves in Fig. 10. The areas between these curves represent the target configuration sets for each rectangle. Following the discussion in Section II, the result of CBTA of the rectangular channel shown in Fig. 9 is the pair of maps $\underline{\alpha}_1$ and $\bar{\alpha}_1$ shown in Fig. 10(a). For every point $W = (0, w)$ on the entry segment of R_1 , and every angle $\alpha \in [\underline{\alpha}_1(w), \bar{\alpha}_1(w)]$, there exists a curvature-bounded path that traverses the entire rectangular channel. Note that these coordinates are in the axes system attached to R_1 , as shown in Fig. 2.

In contrast, the state-of-the-art result on narrow-channel traversals [4] provides no useful information about the traversability of the channel shown in Fig. 9. Specifically, the result in [4] states that the curvature-bounded traversal of a channel (for a uniform curvature bound r^{-1}) is guaranteed if the width w of the channel satisfies $w \geq \tau r$, where $\tau \approx 1.55$, but provides no information about traversal if the width of the channel violates the aforesaid condition. For the example in Fig. 9, this condition is indeed violated. As previously stated, not only does the proposed technique determine the traversability of the channel, but it also considers nonuniform channel width, and nonuniform curvature constraints, neither of which are addressed in [4].

Example 2: To illustrate the practical significance of CBTA for robot motion planning, we briefly discuss its application in simplifying motion planning for vehicles with dynamical constraints. As discussed in Section I-C, motion-planning algorithms based on square or rectangular cell decompositions (cf., [15]) repeatedly invoke a lower level trajectory generation algorithm that finds control inputs to enable the vehicle's traversal through a finite sequence of rectangles (namely, through rectangular channels). MPC [23] is often used for trajectory generation. For example, the motion-planning technique discussed in [15] requires the solutions of trajectory generation problems defined over sequences of length $H + 2$ of square cells, with each square of possibly different dimension, where $H = 1, 2, \dots$

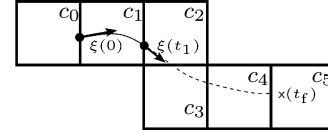


Fig. 11. Tile motion-planning problem with $H = 4$.

To illustrate the application of CBTA in simplifying this trajectory generation problem, we consider the model of a point-mass vehicle subject to acceleration constraints. The dynamical model is described by the differential equations

$$\dot{x}(t) = v(t) \cos \theta(t), \quad \dot{y}(t) = v(t) \sin \theta(t) \quad (3)$$

$$\dot{\theta}(t) = u_2(t), \quad \dot{v}(t) = u_1(t) \quad (4)$$

where x, y denote the inertial position coordinates of the particle, θ is the heading, $v > 0$ is the forward speed, u_1 is the acceleration input, and u_2 is the steering input. The speed v is constrained to lie within prespecified bounds v_{\min} and v_{\max} . The set of admissible control inputs is defined by $U := \left\{ (a, \omega) : (v\omega/f_r^{\max})^2 + (a/f_t^{\max})^2 \leq 1 \right\}$, where f_r^{\max} and f_t^{\max} are prespecified. The input constraint is an example of a “friction ellipse” constraint that models the limited tire frictional forces available for acceleration and steering of the vehicle. In what follows, we denote by $x = (x, y)$ the position vector of the particle and by $\xi = (x, y, \theta, v)$ the state vector.

Let $\{c_0, \dots, c_{H+1}\}$ denote a sequence of geometrically adjacent square cells, i.e., c_k defines a square region for $k = 0, \dots, H + 1$, and this sequence of cells is a rectangular channel, as illustrated in Fig. 11. Let d_k denote the size of the cell c_k , and let x_k^c denote the coordinates of the center of the cell c_k , for $k = 0, \dots, H + 1$. Consider the problem of finding inputs u_1 and u_2 , and a time t_f , if these exist, such that

$$(u_1(t), u_2(t)) \in U \quad \text{for all } t \in [0, t_f] \quad (5)$$

$$x(t) \in \bigcup_{k=1}^H c_k \quad \text{for all } t \in [0, t_f] \quad (6)$$

$$x(t_f) \in c_H \cap c_{H+1} \quad (7)$$

with $x(0) \in c_0 \cap c_1$. The objective of this problem, called the *tile motion-planning problem* [15], is to find control inputs that enable traversal of the particle through the cell c_1 , i.e., to determine the control inputs $u_1, u_2 : [0, t_1] \rightarrow U$, where t_1 is a time instant such that $x(t_1) \in c_1 \cap c_2$. The tile motion-planning problem is a low-level trajectory generation problem that can enable a higher level search algorithm, such as the algorithm described in [15], to find dynamically feasible motion plans. In Fig. 11, the trajectory to be generated is indicated by the solid black curve within cell c_1 , whereas the dotted curve indicates the requirement of satisfying constraint (6). Note that it suffices to guarantee that the trajectory indicated by the dotted curve exists, whereas the trajectory indicated by the solid curve must be determined.

MPC is one approach to the solution of constrained trajectory generation problems, such as the tile motion-planning problem. The main difficulty in the implementation of MPC to solve the preceding trajectory generation problem is that constraint (6) involves, in general, a nonconvex region in the workspace (namely, the interior of the rectangular channel defined by the cells $\{c_1, \dots, c_H\}$).

This difficulty with the implementation of MPC can be mitigated using the proposed CBTA as follows. MPC algorithms can easily incorporate terminal set constraints, i.e., constraints that require the terminal state to lie within a prespecified set. Consider the following reformulation of the tile motion-planning problem: Find inputs \tilde{u}_1, \tilde{u}_2 , and a

TABLE II
SAMPLES OF TILE MOTION-PLANNING EXECUTION TIMES USING MPC

H	Time w/o CBTA (s)	Time with CBTA (s)	Speed-up due to CBTA (ratio)
5	1.672	0.1688	9.909
6	1.782	0.2432	7.327
7	3.621	0.2218	16.33
8	2.022	0.2030	9.959
9	3.283	0.2206	14.88

time t_1 such that

$$(\tilde{u}_1(t), \tilde{u}_2(t)) \in U \quad \text{for all } t \in [0, t_1] \quad (8)$$

$$x(t) \in c_1 \quad \text{for all } t \in [0, t_1] \quad (9)$$

$$\xi(t_1) \in \mathcal{X}_1 \quad (10)$$

where $\mathcal{X}_1 \in c_1 \cap c_2$ is a so-called *effective target set* defined such that for every state $\xi \in \mathcal{X}_1$, there exist control inputs $u_1, u_2 : [t_1, t_f] \rightarrow U$ such that constraints (5)–(7) are satisfied. The advantage of this reformulation of the tile motion-planning problem is that (9) is a convex constraint. However, this advantage is achieved at the expense of introducing constraint (10), which in turn introduces the problem of computing the effective target set \mathcal{X}_1 . Here, the proposed CBTA technique is beneficial, because it efficiently computes the set $\mathcal{X}_1 \cap (\mathbb{R}^2 \times \mathbb{S}^1)$. Notice that the set $\mathcal{X}_1 \cap (\mathbb{R}^2 \times \mathbb{S}^1)$ is, by definition, a target configuration set that was previously discussed in Section II-A. Constraint (10) can be convexified by replacing \mathcal{X}_1 by an interior convex set $\tilde{\mathcal{X}}_1 \subseteq \mathcal{X}_1$. Furthermore, mathematical details of an MPC implementation for this tile motion-planning algorithm based on such a CBTA-based simplification, are available in [20].

To further illustrate the computational benefits enabled by CBTA in the MPC implementation of the tile motion-planning problem, we performed numerical simulations of the tile motion-planning problem on several channels of the form shown in Fig. 11 with different values of H . Sample results of computational time required for the solution of the tile-motion planning problem, with and without the previously mentioned convexification enabled by CBTA, are shown in Table II. All simulations were performed in MATLAB on a computer with an Intel Core i7-860 processor, operating at 2.80 GHz with 16 GB of memory. Whereas we did not find a clear trend of reduction in computation time with increasing values of H , we consistently observed reductions by an order of magnitude.

IV. CONCLUSION

In this paper, we have discussed the geometric problem of CBTA of a polygonal region, namely, *rectangular channels*, formed by a sequence of rectangles with disjoint interiors. More precisely, we proposed the CBTA for establishing the existence of a differentiable curve lying within a given rectangular channel, such that it satisfies an upper bound on its curvature. We proposed a recursive numerical solution of this CBTA problem based on the traversability analysis of a single rectangle. We demonstrated via illustrative examples the significant benefits of the proposed technique over comparable state-of-the-art results from the literature.

We also discussed the application of CBTA for motion planning of autonomous mobile vehicles. Specifically, we discussed the crucial role of CBTA in the transformation of difficult trajectory generation problems subject to dynamical constraints into easier geometric path-planning problems. The proposed CBTA is suitable for online real-time implementations because it involves simple algebraic calculations. Fu-

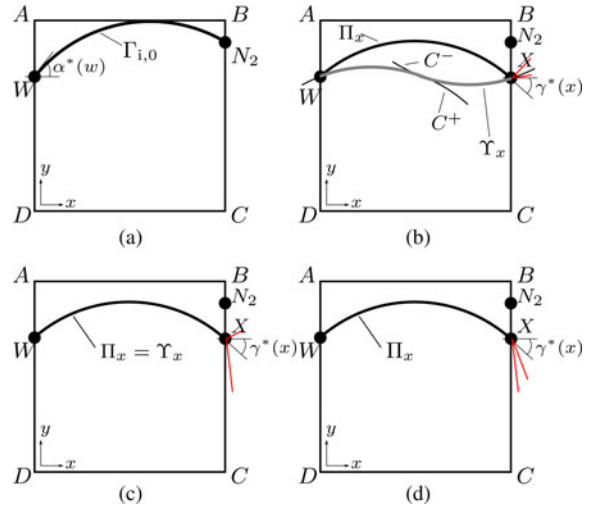


Fig. 12. Geometric considerations in the construction of Υ_x for CBTA-S1.

ture extensions of this study include CBTA with asymmetric constraints on the curvature for left and right turns.

APPENDIX

As discussed in Section II-B, the proposed solutions to CBTA-S1 and CBTA-S2 are based on constructions of the paths Λ_x and Υ_x that satisfy properties P1)–P5). These constructions are based on concatenations of circular arcs and straight line segments, based on the following result.

Lemma A.1 (Boissonnat et al. [10]): If there exists an admissible² path of curvature at most r^{-1} , then there exists an admissible path consisting of a concatenation of straight line segments and arcs of circles of radius r .

In what follows, we will denote by C^+ a clockwise circular arc, by C^- a counterclockwise circular arc, and by S a straight line segment. When necessary, we will denote by C_u^+ , C_u^- , or S_u an arc of length u . To construct the family of paths Υ_x underlying the procedure described in Fig. 4, we use of the following preliminary technical results.

Lemma A.2: If $2r(d-w) \leq d^2 + (d-w)^2$, then the maximum possible tangent angle at $W = (0, w)$ for any Type 1 path is given by $\alpha^*(w)$, which is defined by

$$\alpha^*(w) := \cos^{-1}(1 - (d-w)/r). \quad (A.1)$$

Proof: See [17, pp. 146–147]. ■

Lemma A.3: Let X be a point on the segment YZ . If there exists a Type 1 C^+ path $\Gamma_{i,0}$ between W and X , then the tangent angle at W of any Type 1 path between W and X is no greater than $\Gamma'_{i,0}(W)$.

Proof: See [17, p. 152]. ■

Corollary A.1: If there exists a Type 1 C^+ path $\Gamma_{i,0}$ between W and X , then the tangent angle at X of any Type 1 path between W and X is no less than $\Gamma'_{i,0}(X)$.

Suppose that $2r(d-w) \leq d^2 + (d-w)^2$, and consider the C^+ arc $\Gamma_{i,0}$ that passes through W with $\Gamma'_{i,0}(W) = \alpha^*(w)$. Let $N_2 = (d, n_2)$ be the point of intersection of $\Gamma_{i,0}$ with line BC [see Fig. 12(a)]. It can be shown that n_2 is given by line 3 of the procedure in Fig. 4. It follows that for any point X on the segment N_2Z , there exists no Type 1 admissible path from W to X . It can also be shown that if

²In [10], the term “admissible” defines a curvature-bounded continuously differentiable path that satisfies specified initial and terminal conditions and is contained within a specified polygon.

$2r(d-w) > d^2 + (d-w)^2$, the point of tangency of $\Gamma_{1,0}$ to the line passing through segment AB lies outside the segment AB , and hence, there exists a C^+ arc from W to every point on the segment BC . These observations underlie lines 2–5 of the procedure in Fig. 4.

Next, let $X = (d_1, x)$ be a point such that $x \in [y, n_2] \cap [y, z]$, and let Π_x be the C^+ path between W and X . The existence of this path is guaranteed by the choice of the point N_2 and by the earlier assumption of $r > d$. Let $\gamma^*(x) := \Pi'_x(X)$. It can be shown using elementary geometric arguments that $\gamma^*(x)$ satisfies (3). We consider the following cases of relations between $\gamma^*(x)$ and the angles $\underline{\beta}(x)$ and $\overline{\beta}(x)$:

- 1) $\gamma^*(x) < \underline{\beta}(x)$: Π_x is not a Type 1 path. Define Υ_x as the $C^+ C^-$ path from W to X that satisfies $\Upsilon'_x(X) = \underline{\beta}(x)$ [see Fig. 12(b)]. It can be shown that Υ_x is a Type 1 path and that $\Upsilon'_x(W)$ satisfies (4).
- 2) $\underline{\beta}(x) \leq \gamma^*(x) < \overline{\beta}(x)$: Π_x is a Type 1 path [see Fig. 12(c)], and we identify $\Upsilon_x = \Pi_x$. It can be shown that $\Upsilon'_x(W)$ satisfies (5).
- 3) $\overline{\beta}(x) < \gamma^*(x)$: Π_x is not a Type 1 path, and furthermore, by Corollary A.1, there exists no Type 1 path between W and X [see Fig. 12(d)].

The preceding constructions of Υ_x underlie the calculations in lines 6–12 of the procedure described in Fig. 4. The proofs that these constructions of Υ_x indeed satisfy the properties P1)–P5) described in Section II are based on purely geometric arguments, and the details are available in [17, App. C].

REFERENCES

- [1] H. Choset, K. Lynch, S. Hutchinson, G. Kantor, W. Burgard, L. Kavraki, and S. Thrun, *Principles of Robot Motion: Theory, Algorithms, and Implementations*. Cambridge, MA, USA: MIT Press, 2005.
- [2] S. Fortune and G. Wilfong, "Planning constrained motion," *Ann. Math. Artif. Intell.*, vol. 3, pp. 21–82, 1991.
- [3] H.-K. Ahn, O. Cheong, J. Matousek, and A. Vigneron, "Reachability by paths of bounded curvature in convex polygons," in *Proc. 16th Annu. Symp. Comput. Geom.*, Clear Water Bay, Kowloon, Hong Kong, Jun. 12–14 2000, pp. 251–259.
- [4] S. Bereg and D. Kirkpatrick, "Curvature-bounded traversals of narrow corridors," in *Proc. 21st Annu. Symp. Comput. Geom.*, Pisa, Italy, 2005, pp. 278–287.
- [5] L. E. Dubins, "On curves of minimal length with a constraint on average curvature, and with prescribed initial and terminal positions and tangents," *Amer. J. Math.*, vol. 79, no. 3, pp. 497–516, Jul. 1957.
- [6] X.-N. Bui, J.-D. Boissonnat, P. Souères, and J.-P. Laumond, "Shortest path synthesis for dubins non-holonomic robot," in *Proc. IEEE Int. Conf. Robot. Autom.*, San Diego, CA, USA, May 1994, pp. 2–7.
- [7] J. Reif and H. Wang, "The complexity of the two dimensional curvature-constrained shortest-path problem," in *Proc. Third Workshop Algorithmic Found. Robot.*, 1998, pp. 49–58.
- [8] P. Jacobs and J. Canny, "Nonholonomic Motion Planning," in *Planning Smooth Paths for Mobile Robots*. Norwell, MA, USA: Kluwer, 1992, pp. 271–342.
- [9] P. K. Agarwal and H. Wang, "Approximation algorithms for curvature-constrained shortest paths," *SIAM J. Comput.*, vol. 30, no. 6, pp. 1739–1772, 2001.
- [10] J.-D. Boissonnat, S. K. Ghosh, T. Kavitha, and S. Lazard, "An algorithm for computing a convex and simple path of bounded curvature in a simple polygon," *Algorithmica*, vol. 34, pp. 109–156, 2002.
- [11] J. Backer and D. Kirkpatrick, "Finding curvature-constrained paths that avoid polygonal obstacles," in *Proc. 23rd Annu. Symp. Comput. Geom.*, Gyeongju, Korea, 2007, pp. 66–73.
- [12] T. Fraichard and A. Scheuer, "From Reeds and Shepp's to continuous curvature paths," *IEEE Trans. Robot.*, vol. 20, no. 6, pp. 1025–1035, Dec. 2004.
- [13] K. Yang and S. Sukkarieh, "Real-time continuous curvature path planning of UAVs in cluttered environments," in *Proc. Fifth Int. Symp. Mechatron. Appl.*, May 2008, pp. 1–6.

- [14] E. Bakolas and P. Tsiotras, "On the generation of nearly optimal, planar paths of bounded curvature and bounded curvature gradient," in *Proc. Amer. Control Conf.*, St. Louis, MO, USA, Jun. 2009, pp. 385–390.
- [15] R. V. Cowlagi and P. Tsiotras, "Hierarchical motion planning with dynamical feasibility guarantees for mobile robotic vehicles," *IEEE Trans. Robot.*, vol. 28, no. 2, pp. 379–395, Apr. 2012.
- [16] R. V. Cowlagi and P. Tsiotras, "On the existence and synthesis of curvature-bounded paths inside nonuniform rectangular channels," in *Proc. Amer. Control Conf.*, Baltimore, MD, USA, Jun. 30–Jul. 2, 2010, pp. 5382–5387.
- [17] R. V. Cowlagi, "Hierarchical motion planning for autonomous aerial and terrestrial vehicles," Ph.D. dissertation, Dept. Aerosp. Eng., Georgia Inst. Technol., Atlanta, GA, USA, 2011.
- [18] E. Velenis, P. Tsiotras, and J. Lu, "Optimality properties and driver input parametrization for trail-braking cornering," *Eur. J. Control*, vol. 4, pp. 308–320, 2008.
- [19] J.-H. Jeon, R. V. Cowlagi, S. C. Peters, S. Karaman, E. Frazzoli, P. Tsiotras, and K. Iagnemma, "Optimal motion planning with the half-car dynamical model for autonomous high-speed driving," presented at the Amer. Control Conf., Washington, DC, USA, 2013.
- [20] R. V. Cowlagi and P. Tsiotras, "Hierarchical motion planning with kinodynamic feasibility guarantees: Local trajectory planning via model predictive control," in *Proc. IEEE Int. Conf. Robot. Autom.*, St. Paul, MN, USA, May 14–18 2012, pp. 4003–4008.
- [21] S. J. Anderson, S. B. Karumanchi, and K. Iagnemma, "Constraint-based planning and control for safe, semi-autonomous operation of vehicles," in *Proc. Intell. Veh. Symp.*, Alcalá de Henares, Spain, Jun. 3–7, 2012, pp. 383–388.
- [22] R. Alterovitz, M. Branicky, and K. Goldberg, "Motion planning under uncertainty for image-guided medical needle steering," *Int. J. Robot. Res.*, vol. 27, no. 11–12, pp. 1361–1374, 2008.
- [23] J. M. Maciejowski, *Predictive Control With Constraints*. Englewood Cliffs, NJ, USA: Prentice-Hall, 2002.

On Intensity-Based Nonmetric Visual Servoing

Geraldo Silveira

Abstract—This paper considers the problem of vision-based robot stabilization where the equilibrium state is defined via a reference image. Differently from most solutions, this study directly exploits the pixel intensities with no feature extraction or matching and uses only nonmetric information of the observed scene. Intensity-based techniques provide higher accuracy, whereas not requiring metric information increases their versatility. In this context, this paper further exploits the epipolar geometry and its intrinsic degeneracies. Such degeneracies always occur when that stabilization is sufficiently close to the equilibrium, regardless of the object shape. This remarkable fact allows the development of new vision-based control strategies with varying degrees of computational complexity and of prior knowledge. Importantly, they are arranged hierarchically from the simplest to the state-of-the-art ones, all in a unified framework. Three new local methods are then presented, and their closed-loop performances are experimentally assessed using both planar and nonplanar objects, under small and large displacements, simulating and employing a six-degree-of-freedom robotic arm.

Manuscript received June 13, 2013; revised December 31, 2013; accepted April 1, 2014. Date of publication May 7, 2014; date of current version August 4, 2014. This paper was recommended for publication by Associate Editor R. Eustice and Editor B. J. Nelson upon evaluation of the reviewers' comments.

The author is with the Center for Information Technology Renato Archer (CTI), Division of Robotics and Computer Vision (DRVC), CEP 13069-901 Campinas, Brazil (e-mail: Geraldo.Silveira@cti.gov.br).

This paper has supplementary downloadable material available at <http://ieeexplore.ieee.org>.

Color versions of one or more of the figures in this paper are available online at <http://ieeexplore.ieee.org>.

Digital Object Identifier 10.1109/TRO.2014.2315712